A high speed single side band generator using a magnetic tunnel junction based spin torque nano oscillator

Raghav Sharma,[*,†] Naveen Sisodia,[†] Ezio Iacocca,[‡,¶] A. A. Awad,[§] Johan Åkerman,[§,‖] and P.K Muduli[*,†]

†*Department of Physics, Indian Institute of Technology, Hauz Khas, New Delhi-110016, India*

‡*Division for Theoretical Physics, Chalmers University of Technology, 41296, Gothenburg, Sweden*

¶*Department of Applied Mathematics, University of Colorado, Boulder, Colorado 80304-0526, USA*

§*Department of Physics, University of Gothenburg, 41296, Gothenburg, Sweden*

‖*Materials Physics, School of ICT, KTH-Royal Institute of Technology, Electrum 229, 164 40 Kista, Sweden*

E-mail: sharmaraghav66@yahoo.com; muduli@physics.iitd.ac.in

Abstract

A nanopillar of magnetic tunnel junction (MTJ) consisting of two magnetic layers (free and fixed) separated by an oxide barrier can be used as a tunable radio-frequency (RF) generator as well as a RF signal modulator by using the spin transfer torque effect. Due to their nanoscale sizes, these devices are promising for on-chip based technology with significantly simpler circuitry and lower cost of fabrication. Frequency modulation

(FM) is typically achieved in spin torque nano-oscillators (STNOs) by applying both a dc bias and a low frequency RF current, resulting in a spectrum characterized by multiple sidebands symmetrically located about the carrier. Here, we demonstrate a novel scheme of single side band modulation (SSB) phenomena using a MTJ based STNO, which saves transmission bandwidth (as opposed to FM) and in principle should minimize attenuation for wireless communication. Experimentally, successful lower single side band (LSSB) is achieved for a wide range of modulation frequency, $f_m = 50$ MHz-1 GHz. The observed LSSB is determined by intrinsic properties of the device which can be well modeled by non-linear frequency and amplitude modulation formulation and reproduced in macrospin simulations. Moreover, our macrospin simulation results show that the range of modulation current and modulation frequency for the generation of SSB can be controlled by the field-like torque and biasing conditions.

Keywords

Spin torque nano oscillators, single sideband modulation, non linear frequency and amplitude modulation, magnetic tunnel junction

Introduction

Spin torque nano oscillators (STNOs) [1–3] offer great potential for communication applications due to a large frequency tuning range,[4–6] sub-micron footprints [3] and its straightforward integration with semiconductor technology using the same processes as magnetoresistive random access memory.[7,8] Whereas metallic spin valve based STNOs face output power limitation, magnetic tunnel junction (MTJ) based STNOs have been shown to enhance this figure-of-merit achieving up to 10 μW,[9] which meets the requirements of commercial applications. Another important advantage of STNOs is their ability to produce a modulated signal upon application of a low radio frequency (RF) signal.[10–20] Different modulation schemes e.g., non-

linear frequency modulation (NFM),[21,22] non linear frequency and amplitude modulation (NFAM),[20,23,24] amplitude shift keying (ASK) or on-off keying (OOK) modulation,[25–27] and frequency shift keying (FSK) modulation[28] have been demonstrated in STNOs for communication applications. Recently, ASK modulation scheme was used to demonstrate wireless communication of STNOs signal[25,26] up to distance of 100 cm. Furthermore, Oh *et. al.,*[27] showed the transmission of wireless signals through OOK where different STNOs operating at different frequencies can serve as separate channels for transmission through direct RF-frequency division multiplexing (FDM) techniques. This demonstration provides an initial breakthrough in the field of signal transmission especially digital signal processing using nano-sized STNOs.

In many wireless communication applications the primary baseband signal is naturally generated in the form of analog signal, such as voice or audio signals, and additional circuitry is required for the analog-to digital conversion. This increases the complexity of the circuit. STNOs can be directly used as an analog frequency modulator.[16,20,21] However, analog frequency modulation schemes requires twice the bandwidth of the original baseband signal and consumes high power due to transmission of both lower and upper sidebands. Besides, such analog frequency modulation scheme suffers from higher attenuation in long-haul communication and telemetering circuits particularly those which include several by-pass points. The international telecommunication union (ITU) has recommended to use broadcasting with single side band (SSB) modulation. It is hence desired that all form of communication be based on SSB. The SSB modulation requires less power to transmit than conventional amplitude modulation (AM) and needs only one half of the bandwidth required in other modulation schemes like double sideband suppressed carrier (DSB-SC). Compared to popular vestigial sideband (VSB) modulation scheme, SSB utilizes 25% less bandwidth for the transmission. SSB modulation is used for long distance transmission because it allows longer spacing between repeaters. However, traditional SSB modulators e.g., Hartley modulator[29] or Weaver modulator[30] require many circuit components such as low pass filters, phase

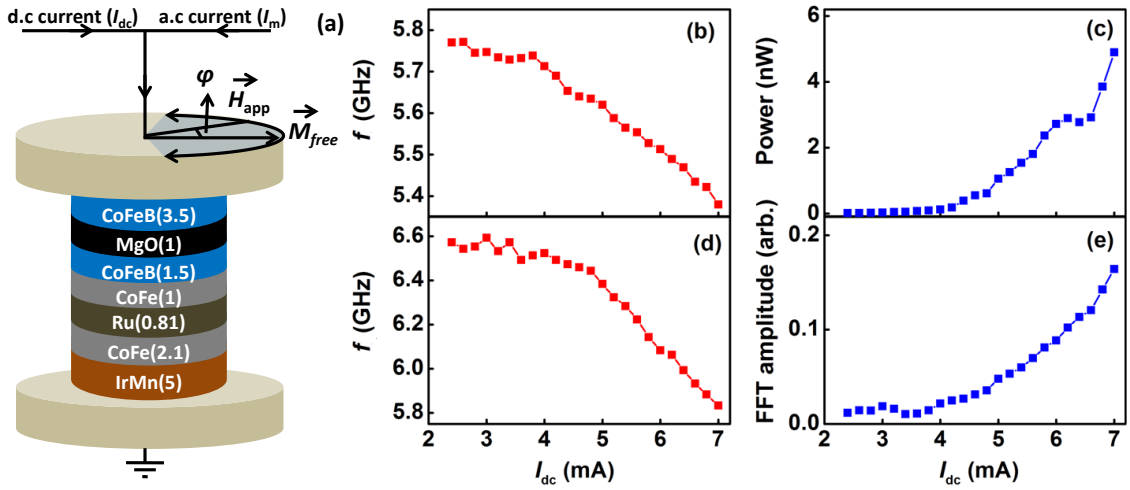

Figure 1: The device structure and free running properties. (a) The magnetic tunnel junction based device consists of a bottom pinned layer (PL), a reference layer (RL), a MgO barrier and the top CoFeB free layer (FL). The PL is composed of IrMn(5 nm)/CoFe (2.1 nm)/Ru(0.81 nm), where as the RL is composed of CoFe(1 nm)/CoFeB(1.5 nm). (b) Frequency and (c) Power vs d.c. current (in the absence of any RF current) measured at $H_{app} = 450$ Oe, $\varphi = 190°$. (d) and (e) are the simulation results at the same experimental conditions and at $T = 300$ K.

shifter and quadrature mixers. This significantly increases both size and complexity of the modulators.

Here, we propose an entirely new way for SSB modulation, where a sub-micron sized-STNO device is used to directly generate a SSB modulated signal with a high carrier frequency. We demonstrate lower single side band (LSSB) data modulation rate up to 1 GHz taking advantage from the STNO's non-linear properties. This advancement in SSB through STNOs opens up a new dimension of application which is easily approachable, fast and practical for the on-chip based technology. We show that observed SSB can be quantitatively explained using the NFAM theory.[20,23,24] Furthermore, using macrospin simulations we show that the field like torque can be used to manipulate the range of modulation current, I_m and modulation frequency f_m for observing the SSB.

Results and discussion

The device is based on a nanopillar of MTJ–based STNO as shown in Fig.1 (a). The structure of the device is composed of IrMn(5 nm)/CoFe (2.1 nm)/Ru(0.81 nm)/CoFe(1 nm)/CoFeB(1.5 nm)/MgO(1 nm)/ CoFeB (3.5 nm). The antiferromagnetic IrMn layer is used to provide an exchange bias on the adjacent CoFe-pinned layer (PL), which couples antiferromagnetically through Ru to the composite CoFe/CoFeB reference layer (RL). The CoFeB layer above the MgO tunnel barrier is the free layer (FL). The RL magnetization is taken to be along the positive x-axis. The magnetization of the FL at zero field is antiparallel to the magnetization of the RL, so that the angle between the free and reference layer is 180°. The FL can be coherently rotated with an external magnetic field in a range of 140° to 220°.[13] Figures 1(b) and (c) show the behavior of frequency and power versus d.c. current, measured at an in-plane magnetic field $H_{app} = 450$ Oe, and $\varphi = 190°$.[31] As expected for this device,[31] the precession corresponds to the FL for which the frequency red-shifts and power increases very rapidly with d.c. current. Figures 1 (d) and (e) show the corresponding simulated behavior of the FL frequency and power versus d.c. current. The simulated behavior (see methods) qualitatively reproduces the free running STNO. An important property of this free-running behavior is the presence of a maximum frequency of the operation of STNO, $f_{\max} \sim 5.74$ GHz for experimental data and ∼6.57 GHz for simulated data.

In Fig. 2, we show how a lower single side band (LSSB) modulation is produced, when an additional RF signal is superimposed with the d.c.current. The additional RF signal with relatively low frequency is analogous to the information that needs to be sent with the high frequency carrier generated by the STNO. The LSSB generation is shown in Fig. 2(a-c) and Fig. 2(d-f) at varying modulation current and modulation frequency, respectively. The LSSB generation is characterized by dramatic disappearance of the upper sideband in the spectrum. Figure 2 (a) shows the example spectra at I_{dc}=4.4 mA for different modulation currents, showing only the lower sideband. Figure 2 (b-c) shows the frequency spectrum as a function of I_m at $f_m = 500$ MHz for two example of d.c biasing currents of $I_{dc} = 4.4$ mA

and I_{dc} = 6.4 mA, which corresponds to two different regimes of operation of the MTJ-STO. Fig. 2(d) shows the spectra at I_{dc} = 4.4 mA for different f_m whereas Figs. 2(e-f) shows the frequency spectrum for $f_m = 120 - 500$ MHz at I_m = 1.2 mA at d.c biasing currents of $I_{dc} = 4.4$ mA and $I_{dc} = 6.4$ mA. The threshold current (I_{th}) for auto oscillations in this device is about 6.2 mA.[32,33] Hence I_{dc} = 4.4 mA is in the sub-threshold region, where as I_{dc} = 6.4 mA is in above the threshold region. The signals obtained at 4.4 mA is attributed to thermally driven ferromagnetic resonance signals.[2] Hence, the power of the carrier and sidebands in case of $I_{dc} = 4.4$ mA is much less than $I_{dc} = 6.4$ mA. For the case of I_{dc} = 4.4 mA, LSSB is obtained for the entire range of measured $f_m = 100 - 500$ MHz [Fig. 2 (c)], whereas for I_{dc} = 6.4 mA, LSSB is obtained for $f_m > 275$ MHz [Fig. 2 (f)] at $I_m = 1.2$ mA. For the condition of $I_{dc} = 4.4$ mA, STNO is modulated close to $f_{\max}$ as shown in Fig. 1 (b) for $f_m = 100 - 500$ MHz, so that the frequency of the upper sideband falls in the region of frequency where no mode is allowed. This leads to generation of LSSB modulation. However, for the case of $I_{dc} = 6.4$ mA, carrier frequency is far from $f_{\max}$ which explains the reason of higher threshold $f_m = 275$ MHz for observation of clear LSSB modulation. Hence the operating region of SSB strongly depends on the value of d. c. current and operating above I_{th} shifts the onset of SSB to higher f_m for a given I_m . The onset of SSB increases to 350 MHz at $I_{dc} = 7$ mA for $I_m = 1.2$ mA.

The behavior of LSSB modulation has been reproduced by macrospin simulations as shown in Fig. 3. Similar to the experimental conditions, we have selected two bias current conditions from Fig.1 (c). These conditions are I_{dc} = 5 mA and 6.4 mA corresponding to sub- threshold region and above threshold regions, respectively. The simulated results show excellent qualitative agreement with the experimental results shown in Fig.2 for the corresponding cases of $I_{dc} = 4.4$ and 6.4 mA. In simulations, we also studied the modulation behavior at much higher bias current of $I_{dc} = 7$ mA, and found that SSB can be achieved at relatively high $f_m = 450$ MHz and low $I_m = 0 - 1.2$ mA. In fact, the onset f_m where a clear SSB can be seen above threshold current increases with the increase in I_{dc} in agreement with

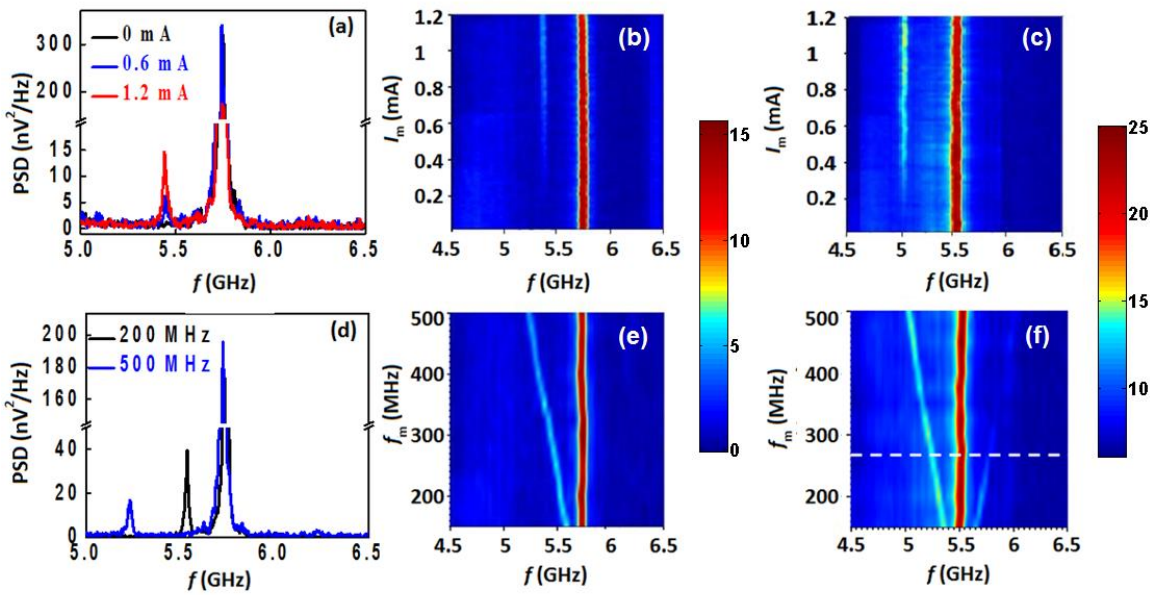

Figure 2: Lower single side band modulation. (a) Example spectra showing single side band modulation at $I_{dc} = 4.4$ mA for different modulation currents. Map of power vs frequency and modulation current at (b) $I_{dc} = 4.4$ mA and (c) $I_{dc} = 6.4$ mA. (d) Example spectra showing single side band modulation at $I_{dc} = 4.4$ mA for different modulation frequencies. Map of power vs frequency and modulation frequency at (e) $I_{dc} = 4.4$ mA and (f) $I_{dc} = 6.4$ mA. The white dashed lines in (f) separates the region of NFAM and LSSB.

experiment.

The generation of LSSB with complete suppression of upper sideband is a very striking observation. We will show below that it is a consequence of combined non-linear frequency and amplitude modulation (NFAM).[34] The NFAM theory predicts unequal amplitude of sidebands and has been successfully applied to nano-contact based STNOs.[16,21] In Fig.4 (a & b) we show the experimental behavior of the power of the carrier and first order sidebands with modulation current for two values $f_m = 200$ MHz for $I_{dc} = 4.4$ mA and 6.4 mA, respectively. As can be seen the upper sideband has significantly lower power than the lower sideband.

We will now explain the behavior of the power of the carrier and sidebands with modulation current using NFAm theory. Assuming that the frequency is non-linear up to 4th order

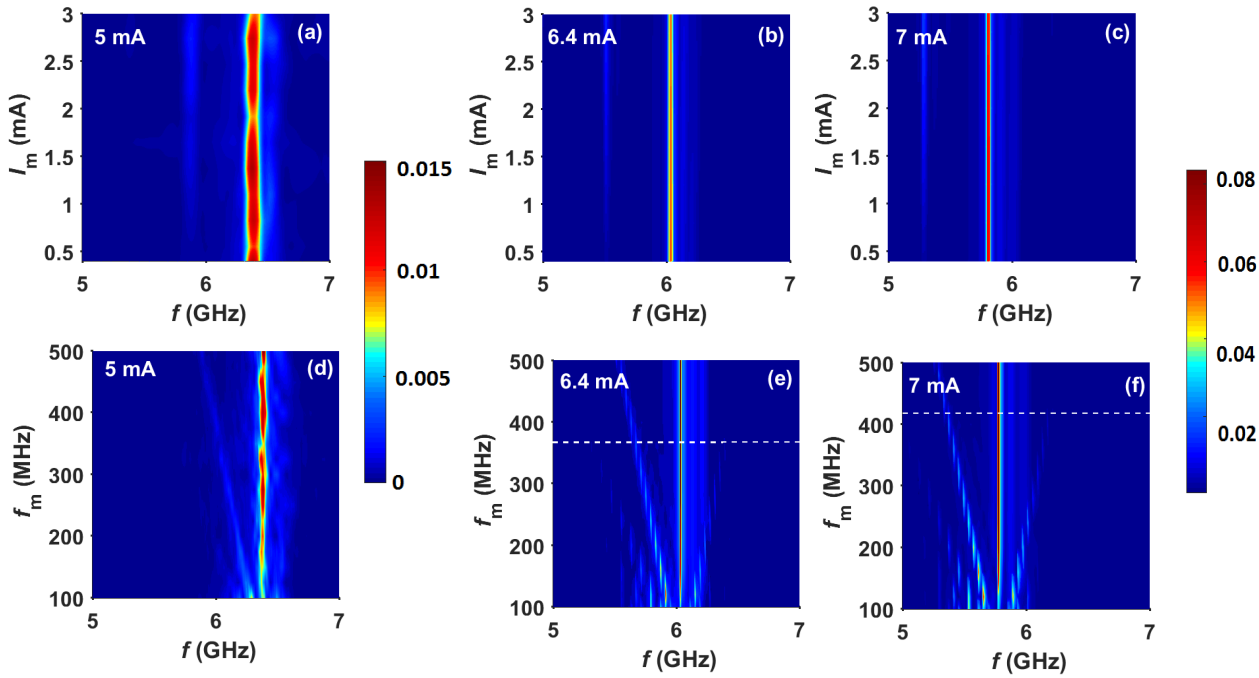

Figure 3: Macrospin simulation results : Map of power vs frequency and modulation current at (a) $I_{dc} = 5$ mA (b) $I_{dc} = 6.4$ mA and (c) $I_{dc} = 7$ mA. Map of power vs frequency and modulation frequency at (d) $I_{dc} = 5$ mA (e) $I_{dc} = 6.4$ mA and (f) $I_{dc} = 7$ mA. The white dashed lines in (e) and (f), separates the region of NFAM and SSB.

and the amplitude is non-linear up to 3rd order, the NFAM spectrum can be written as:[34]

$$\begin{aligned} S(f) =& \frac{1}{4}\sum_{h=0}^{3}\gamma_h \sum_{m,n,p,q=-\infty}^{\infty} J_m(\beta_1)J_n(\beta_2)J_p(\beta_3)J_q(\beta_4) \\ & \big[\delta(f - f_c^I - (n+2m+3p+4q+k)f_m) \\ & + \delta(f - f_c^I - (n+2m+3p+4q-k)f_m) \\ & + \delta(f + f_c^I - (n+2m+3p+4q+k)f_m) \\ & + \delta(f + f_c^I - (n+2m+3p+4q-k)f_m)\big] \end{aligned} \tag{1}$$

where $\beta_1 = k_1 I_m/f_m + 3k_3 I_m^3/4f_m$, $\beta_2 = k_2 I_m^2/4f_m + k_4 I_m^4/4f_m$, $\beta_3 = k_3 I_m^3/12f_m$ and $\beta_4 = k_4 I_m^4/32f_m$ are frequency modulation indices of different order. $\gamma_0 = \lambda_0 + \lambda_2 I_m^2/2$, $\gamma_1 = \lambda_1 I_m + 3\lambda_3 I_m^3/4$, $\gamma_2 = \lambda_2 I_m^2/2$, and $\gamma_3 = \lambda_3 I_m^3/4$ are amplitude modulation parameters. The amplitude modulation (k_i, where i= 1,2,3 and 4) and frequency modulation (λ_i, where

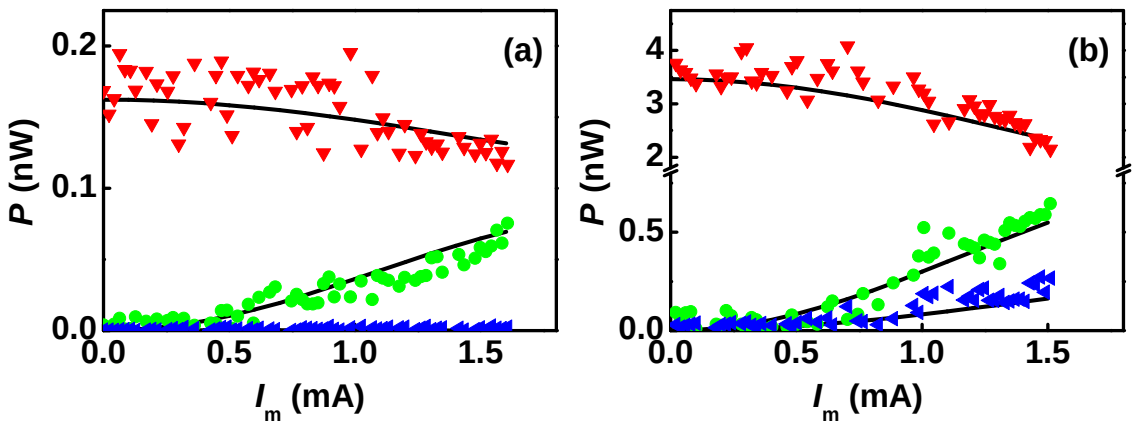

Figure 4: Integrated power of the carrier (red triangles), and the first-order upper (blue squares) and lower (green circles) sidebands for $f_m = 200$ MHz at (a) $I_{dc} = 4.4$ mA and (b) 6.4 mA, respectively. The calculated integrated power as predicted by NFAM are shown by the solid lines.

i= 1,2 and 3) indices are calculated from the fourth and third order polynomial fittings to free running behavior of frequency and amplitude with bias current. These fittings and corresponding calculation of amplitude and frequency modulation indices are shown in the supplementary material.

We keep the range of I_m from $0-1.5$ mA so that modulation acts as a small perturbation. As expected from the modulation theory, the carrier power decreases and the lower and upper sideband power increases with modulation power. Similarly, NFAM theory reflects the same dependence with modulation current I_m; Figs. 4 (a) and (b) as the I_m increases. However, for $I_{dc} = 4.4$ mA the upper sideband is always completely suppressed and only lower side-band is present. Such asymmetric sideband power is a consequence of the STNO's non-linearity and can be fitted by NFAM theory .[16] At $I_{dc} = 6.4$ mA the LSSB power is non-zero at 200 MHz.

In order to further explore the origin of SSB in our experiment, we investigated the influence of field like torque on SSB modulation using macrospin simulations. Figure 5 (a-f) shows the effect of the ratio of field-like torque to spin transfer torque $b_f = 0$, 0.25 and 0.50 for the wide range of $f_m = 40 - 500$ MHz and $I_m = 0.2 - 1.2$ mA. It is clear from the comparison that at higher field-like torque, no clear SSB modulation is observed. At

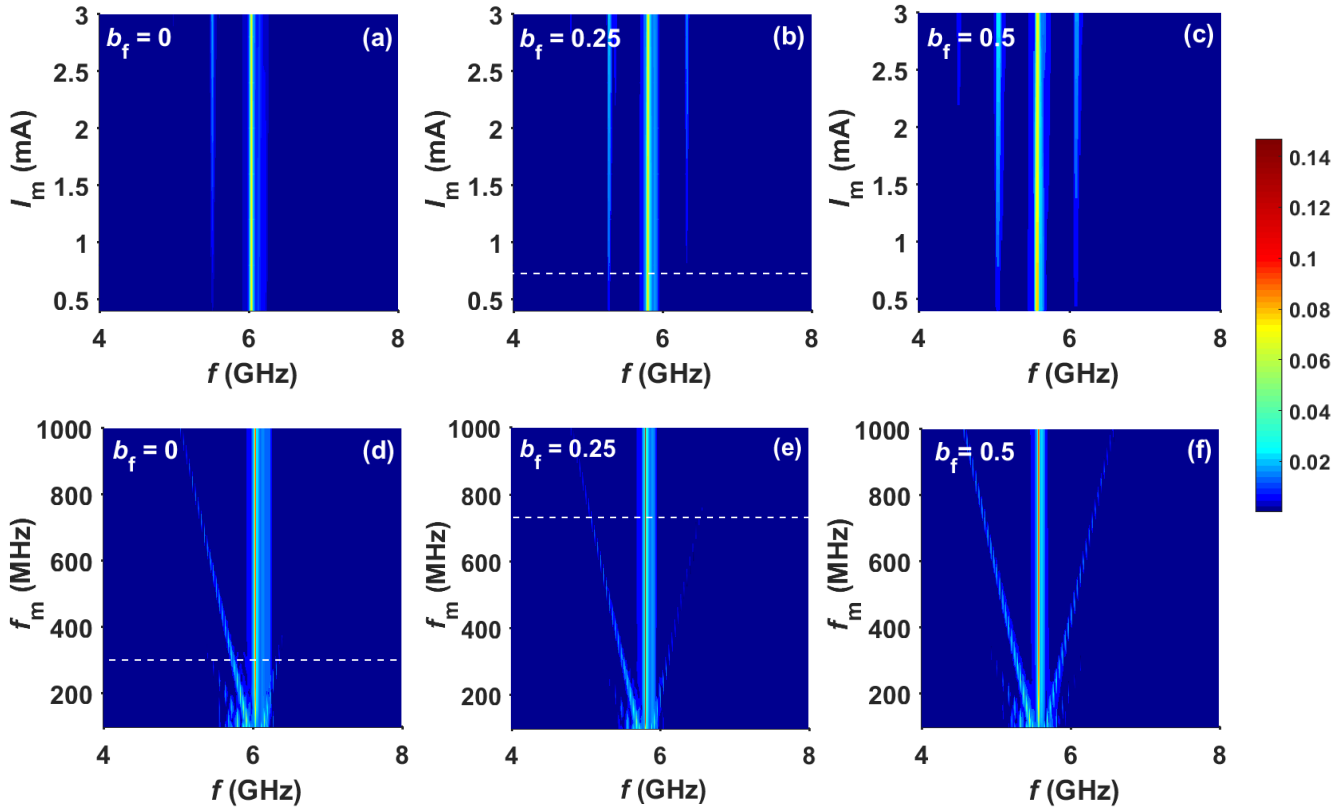

Figure 5: Macrospin simulation results : Map of power vs frequency and modulation current at $I_{dc} = 6.4$ mA for (a) $b_f = 0$, (b) $b_f = 0.25$ and (c) $b_f = 0.5$. Map of power vs frequency and modulation frequency at (d) $b_f = 0$, (e) $b_f = 0.25$ and (f) $b_f = 0.5$. The white dashed lines in (b), (d) and (e), separates the region of NFAM and SSB.

low values of $b_f = 0.10$, the threshold f_m increases drastically from 325 MHz to 800 MHz as compared to the condition of $b_f = 0$. This behavior of LSSB with field-like torque is expected on the basis of following arguments. LSSB is mainly caused by large amplitude non-linearity and weak frequency tunability observed in Fig.1. The field-like term affects the frequency tunability with bias current.[31,35,36] Hence for higher field-like term, the USB frequency can lie below f_{max} with finite power-leading to disappearance of SSB. Thus the observation of SSB in our experimental results indicates the presence of smaller field-like torque, which is consistent with our earlier works on similar devices.[31,37]

Conclusion

In conclusion, the non-linear frequency and amplitude modulation behavior is explored to obtain LSSB modulation in an MTJ- based STNO. We demonstrated SSB for a sub-threshold regime and above threshold regimes at modulation current in the range of 0.3-1.5 mA. Successful LSSB is also achieved for modulation frequencies f_m ranging from 50 MHz to 1 GHz, indicating a robust LSSB modulation of these systems. The performance of the STNOs as a SSB generator can be tuned with operating conditions as well as field-like torque term present in MTJ-based devices. Given the fast data rate, smaller size, and easier implementation, SSB modulation through MTJ based STNOs can potentially meet the demand of much compact and integration on the microchip based communication devices to replace existing complex SSB generators.

Experimental method

The device is a nanopillar with circular cross-section with a nominal diameter of 180 nm. The resistance-area product in the parallel state is about 1.5 μm^2. The modulation current and dc bias current applied simultaneously using a capacitive and inductive port of the bias tee. A resistive microwave power divider (0-12.4 GHz) was used between the bias tee and amplifier to send the modulating signal from an external signal source, a Rohde & Schwarz SMB 100A signal generator. The modulation current was varied from 0 mA to 1.5 mA and the modulation frequency was varied in the range of 50 MHz-1 GHz. The detected signal was amplified and detected in a spectrum analyzer. The amplifier had a gain of 52 dB and working range of $1 - 18$ GHz. All the data are corrected to take into account of the amplification, losses due to the power divider, losses in the transmission line and losses due to reflection at the STNO (impedance mismatch). The reflection due to impedance mismatch is calculated from the scattering matrix element S_{11}, measured with a vector network analyzer.[13] A projected field magnet mounted on a stepper motor was used to vary

the in-plane field angle.

Simulation details

Macrospin simulations were performed by solving the Landau-Lifshitz-Gilbert-Slonczewski (LLGS) equation. Fourth order Runge-Kutta method was used for temporal discretization of LLGS equation which was then integrated in small time steps dt to obtain an approximate numerical solution. The various parameters used for simulation are as follows: saturation magnetization, M_{sat} = 1000 emu/cc ; diameter of the device, t = 240 nm ; polarization efficiency, $P = 0.65$; thickness of the free layer, $t_{fl} = 3.5$ nm; and gilbert Damping parameter, $\alpha = 0.02$. Fixed layer polarization was taken along $\hat{x}$ direction. The device diameter was used as a fitting parameter to match the threshold current with experiments. The parameters used for simulation are similar to our earlier work.[37] To include the effect of temperature, a time varying random field was also introduced in the system which was added to the net effective field. This random noise was scaled numerically using the formulation given by William Fuller Brown.[38] During the simulation, the behavior of magnetization under different external perturbations was recorded in time domain. This data was later converted to the frequency domain using fast fourier transform (FFT) for comparison with obtained experimental results.

Supporting Information Available: Determination of frequency and amplitude modulation sensitivity coefficients from free running properties and macrospin simulation of STNO frequency vs. bias current with varying field-like torque are discussed in the supplementary material.

Acknowledgement

Partial support by the Department of Science and Technology under Fast-Track Scheme and the Department of Electronics and Information Technology (DeitY), Government of India

is gratefully acknowledged. Support from The Swedish Foundation for strategic Research (SSF), The Swedish Research Council (VR), and the Göran Gustafsson Foundation is gratefully acknowledged. Johan Åkerman is a Royal Swedish Academy of Sciences Research Fellow supported by a grant from the Knut and Alice Wallenberg Foundation. Authors thank the IIT Delhi HPC facility for computational resources. Raghav Sharma and Naveen Sisodia acknowledges support from Ministry of Human Resource Development (MHRD), India. Ezio Iacocca acknowledges support from the Swedish Research Council, Reg. No. 637-2014-6863.

References

1. Kiselev, S. I.; Sankey, J. C.; Krivorotov, I. N.; Emley, N. C.; Schoelkopf, R. J.; Buhrman, R. A.; Ralph, D. C. Microwave oscillations of a nanomagnet driven by a spin-polarized current. *Nature* **2003**, *425*, 380–383.

2. Deac, A. M.; Fukushima, A.; Kubota, H.; Maehara, H.; Suzuki, Y.; Yuasa, S.; Nagamine, Y.; Tsunekawa, K.; Djayaprawira, D. D.; Watanabe, N. Bias-driven high-power microwave emission from MgO-based tunnel magnetoresistance devices. *Nat. Phys.* **2008**, *4*, 803–809.

3. Villard, P.; Ebels, U.; Houssameddine, D.; Katine, J.; Mauri, D.; Delaet, B.; Vincent, P.; Cyrille, M.-C.; Viala, B.; Michel, J.-P. *et al.* A GHz Spintronic-Based RF Oscillator. *IEEE J. Solid-State Circuits* **2010**, *45*, 214–223.

4. Rippard, W.; Pufall, M.; Kaka, S.; Russek, S.; Silva, T. Direct-current induced dynamics in C o 90 F e 10/N i 80 F e 20 point contacts. *Phys. Rev. Lett.* **2004**, *92*, 027201.

5. Bonetti, S.; Tiberkevich, V.; Consolo, G.; Finocchio, G.; Muduli, P.; Mancoff, F.; Slavin, A.; Åkerman, J. Experimental evidence of self-localized and propagating spin

wave modes in obliquely magnetized current-driven nanocontacts. *Phys. Rev. Lett.* **2010**, *105*, 217204.

6. Ralph, D. C.; Stiles, M. D. Spin transfer torques. *J. Magn. Magn. Mater.* **2008**, *320*, 1190–1216.

7. Åkerman, J. Toward a universal memory. *Science* **2005**, *308*, 508–510.

8. Dave, R. W.; Steiner, G.; Slaughter, J.; Sun, J.; Craigo, B.; Pietambaram, S.; Smith, K.; Grynkewich, G.; DeHerrera, M.; Akerman, J. *et al.* MgO-based tunnel junction material for high-speed toggle magnetic random access memory. *IEEE Trans. Magn.* **2006**, *42*, 1935–1939.

9. Tsunegi, S.; Yakushiji, K.; Fukushima, A.; Yuasa, S.; Kubota, H. Microwave emission power exceeding 10 μ W in spin torque vortex oscillator. *Appl. Phys. Lett.* **2016**, *109*, 252402.

10. Bonetti, S.; Tiberkevich, V.; Consolo, G.; Finocchio, G.; Muduli, P.; Mancoff, F.; Slavin, A.; Åkerman, J. Experimental Evidence of Self-Localized and Propagating Spin Wave Modes in Obliquely Magnetized Current-Driven Nanocontacts. *Phys. Rev. Lett.* **2010**, *105*, 217204.

11. Bonetti, S.; Muduli, P.; Mancoff, F.; Åkerman, J. Spin torque oscillator frequency versus magnetic field angle: The prospect of operation beyond 65 GHz. *Appl. Phys. Lett.* **2009**, *94*, 102507.

12. Rippard, W. H.; Pufall, M. R.; Kaka, S.; Silva, T. J.; Russek, S. E. Current-driven microwave dynamics in magnetic point contacts as a function of applied field angle. *Phys. Rev. B* **2004**, *70*, 100406.

13. Muduli, P. K.; Heinonen, O. G.; Åkerman, J. Intrinsic frequency doubling in a magnetic tunnel junction-based spin torque oscillator. *J. Appl. Phys.* **2011**, *110*, 076102.

14. Pufall, M. R.; Rippard, W. H.; Kaka, S.; Silva, T. J.; Russek, S. E. Frequency modulation of spin-transfer oscillators. *Appl. Phys. Lett.* **2005**, *86*, 082506.

15. Manfrini, M.; Devolder, T.; Kim, J.-V.; Crozat, P.; Zerounian, N.; Chappert, C.; van Roy, W.; Lagae, L.; Hrkac, G.; Schrefl, T. Agility of vortex-based nanocontact spin torque oscillators. *Appl. Phys. Lett.* **2009**, *95*, 192507.

16. Muduli, P. K.; Pogoryelov, Y.; Bonetti, S.; Consolo, G.; Mancoff, F.; Åkerman, J. Nonlinear frequency and amplitude modulation of a nanocontact-based spin-torque oscillator. *Phys. Rev. B* **2010**, *81*, 140408.

17. Muduli, P. K.; Pogoryelov, Y.; Zhou, Y.; Mancoff, F.; Åkerman, J. Spin Torque Oscillators and RF Currents-Modulation, Locking, and Ringing. *Integr. Ferroelectr.* **2011**, *125*, 147–154.

18. Muduli, P. K.; Pogoryelov, Y.; Mancoff, F.; Åkerman, J. Modulation of Individual and Mutually Synchronized Nanocontact-Based Spin Torque Oscillators. *IEEE Trans. Magn.* **2011**, *47*, 1575–1579.

19. Pogoryelov, Y.; Muduli, P. K.; Bonetti, S.; Iacocca, E.; Mancoff, F.; Åkerman, J. Frequency modulation of spin torque oscillator pairs. *Appl. Phys. Lett.* **2011**, *98*, 192501.

20. Pogoryelov, Y.; Muduli, P. K.; Bonetti, S.; Mancoff, F.; Åkerman, J. Spin-torque oscillator linewidth narrowing under current modulation. *Appl. Phys. Lett.* **2011**, *98*, 192506.

21. Pufall, M.; Rippard, W.; Kaka, S.; Silva, T.; Russek, S. Frequency modulation of spin-transfer oscillators. *Appl. Phys. Lett.* **2005**, *86*, 082506.

22. Martin, S.; Thirion, C.; Hoarau, C.; Baraduc, C.; Dieny, B. Tunability versus deviation sensitivity in a nonlinear vortex oscillator. *Phys. Rev. B* **2013**, *88*, 024421.

23. Muduli, P. K.; Pogoryelov, Y.; Bonetti, S.; Consolo, G.; Mancoff, F.; Åkerman, J. Nonlinear frequency and amplitude modulation of a nanocontact-based spin-torque oscillator. *Phys. Rev. B* **2010**, *81*, 140408.

24. Iacocca, E.; Åkerman, J. Analytical investigation of modulated spin-torque oscillators in the framework of coupled differential equations with variable coefficients. *Phys. Rev. B* **2012**, *85*, 184420.

25. Choi, H. S.; Kang, S. Y.; Cho, S. J.; Oh, I. Y.; Shin, M.; Park, H.; Jang, C.; Min, B.; Min, C.; Kimm, S. I. *et al.* Spin nano-oscillator-based wireless communication. *Sci. Rep.* **2014**, *4*, 4586.

26. Sharma, R.; Durrenfeld, P.; Iacocca, E.; Heinonen, O.; Åkerman , J.; Muduli , P. K. Modulation Rate Study in a Spin-Torque Oscillator-Based Wireless Communication System . *Appl. Phys. Lett.* **2015**, *51*, 1401304.

27. Oh, I. Y.; Park, S. Y.; Kang, D. H.; Park, C. S. Wireless spintronics modulation with a spin torque nano-oscillator (STNO) array. *IEEE Microwave and Wireless Comp. Lett.* **2014**, *24*, 502.

28. Manfrini, M.; Devolder, T.; Kim, J.-V.; Crozat, P.; Chappert, C.; Van Roy, W.; Lagae, L. Frequency shift keying in vortex-based spin torque oscillators. *J. Appl. Phys.* **2011**, *109*, 083940.

29. Carson, R., John Method and means for signaling with high-frequency waves. 1923; US Patent 1,449,382.

30. Weaver, D. K. A third method of generation and detection of single-sideband signals. *Proceedings of the IRE* **1956**, *44*, 1703–1705.

31. Muduli, P. K.; Heinonen, O. G.; Åkerman, J. Bias dependence of perpendicular spin

torque and of free- and fixed-layer eigenmodes in MgO-based nanopillars. *Phys. Rev. B* **2011**, *83*, 184410.

32. Muduli, P. K.; Heinonen, O. G.; Åkerman, J. Decoherence and Mode Hopping in a Magnetic Tunnel Junction Based Spin Torque Oscillator. *Phys. Rev. Lett.* **2012**, *108*, 207203.

33. Heinonen, O.; Muduli, P.; Iacocca, E.; Åkerman, J. Decoherence, Mode Hopping, and Mode Coupling in Spin Torque Oscillators. *IEEE Trans. Magn.* **2013**, *49*, 4398–4404.

34. Consolo, G.; Puliafito, V.; Lopez-Diaz, L.; Nizzoli, F.; Giovannini, L.; Valenti, G.; Azzerboni, B. A Generalized Model of Nonlinear Dynamics in Combined Frequency-Amplitude Modulators. *IEEE Trans. Magn.* **2010**, *46*, 3629–3634.

35. Heinonen, O. G.; Stokes, S. W.; Yi, J. Y. Perpendicular Spin Torque in Magnetic Tunnel Junctions. *Phys. Rev. Lett.* **2010**, *105*, 066602.

36. Petit, S.; Baraduc, C.; Thirion, C.; Ebels, U.; Liu, Y.; Li, M.; Wang, P.; Dieny, B. Spin-Torque Influence on the High-Frequency Magnetization Fluctuations in Magnetic Tunnel Junctions. *Phys. Rev. Lett.* **2007**, *98*, 077203.

37. Tiwari, D.; Sisodia, N.; Sharma, R.; Dürrenfeld, P.; Åkerman, J.; Muduli, P. Enhancement of spin-torque diode sensitivity in a magnetic tunnel junction by parametric synchronization. *Appl. Phys. Lett.* **2016**, *108*, 082402.

38. Brown Jr, W. F. Thermal fluctuations of a single-domain particle. *J. Appl. Phys.* **1963**, *34*, 1319–1320.